Fluorescence Phasor Plots Using Time Domain Data: Effect of the Instrument Response Function

ARTICLE *in* THE JOURNAL OF PHYSICAL CHEMISTRY B · JULY 2015

Impact Factor: 3.3 · DOI: 10.1021/acs.jpcb.5b00261 · Source: PubMed

3 AUTHORS:

Liliana Martelo
Technical University of Lisbon
5 PUBLICATIONS **3** CITATIONS
SEE PROFILE

Aleksander Fedorov
Technical University of Lisbon
97 PUBLICATIONS **2,111** CITATIONS
SEE PROFILE

Mario N Berberan Santos
University of Lisbon
200 PUBLICATIONS **3,366** CITATIONS
SEE PROFILE

***J. Phys. Chem. B* in press (2015)**

http://dx.doi.org/10.1021/acs.jpcb.5b00261

Fluorescence Phasor Plots Using Time Domain Data: Effect of the Instrument Response Function

Liliana Martelo, Alexander Fedorov, and Mário N. Berberan-Santos*

CQFM - Centro de Química-Física Molecular and IN - Institute of Nanoscience and Nanotechnology, Instituto Superior Técnico, Universidade de Lisboa, 1049-001 Lisboa, Portugal

*E-mail: berberan@tecnico.ulisboa.pt

ABSTRACT

Phasor plots of the fluorescence intensity decay (plots of the Fourier sine transform vs. the Fourier cosine transform, for one or several angular frequencies) are being increasingly used, namely in fluorescence lifetime imaging microscopy (FLIM) of cells, tissues and surfaces, but are also relevant for the characterization of homogeneous (e.g. solution) systems. In this work, the construction of the phasor plot using time domain data is discussed, including the effect of the instrument response function (IRF). A deconvolution method in the Fourier space is described. The results obtained are applied to fluorescence decays of aqueous fluorescein (basic form) in the presence of concentrated potassium iodide. The effect of the impulse is clearly shown, in accordance with model predictions. Deconvolution in the Fourier space works well for lifetimes at least one order of magnitude higher than the IRF time width.

1. INTRODUCTION

A *luminescence decay function*, $I(t)$, is the function describing the time dependence of the intensity of radiation spontaneously emitted at a given wavelength, by a previously excited sample. Only nonnegative times are considered ($t \geq 0$). For convenience, and without loss of generality, the decay function is usually normalized at $t = 0$, $I(0) = 1$ (initial value normalization).[1,2] A second normalization procedure (area normalization) is to consider instead the function

$$E(t) = \frac{I(t)}{\int_0^\infty I(t)dt}. \tag{1}$$

In this case, $E(t)$ can be called a *density*,[3] as it has the properties of a probability density function (pdf). This definition has the advantage of including "decay" functions that start from zero, as occurs with the emission of intermediates and products of photochemical processes. The function $E(t)$ also has the meaning of the emission probability of a photon between t and $t + dt$, given that the photon was emitted.

The cosine and sine Fourier transforms of $E(t)$, $G(\omega)$ and $S(\omega)$, respectively, are defined by[1,4,5]

$$G[E] = G(\omega) = \int_0^\infty \cos(\omega u)\, E(u)\, \mathrm{d}u, \tag{2}$$

$$S[E] = S(\omega) = \int_0^\infty \sin(\omega u)\, E(u)\, \mathrm{d}u, \tag{3}$$

where ω is the angular frequency. Following Weber,[5] the letter G is used instead of C (G is a convenient choice, as it avoids the concentration symbol while retaining graphic similarity with C).

Each decay function, for a given frequency, is mapped onto a point inside the unit circle defined by $G^2 + S^2 = 1$,[3,6] which may be said to be the *phasor space*, see Figure 1. It also follows from eqs 2 and 3 that $G(0) = 1$ and $S(0) = 0$, while $S(\infty) = G(\infty) = 0$, see Figure 1.

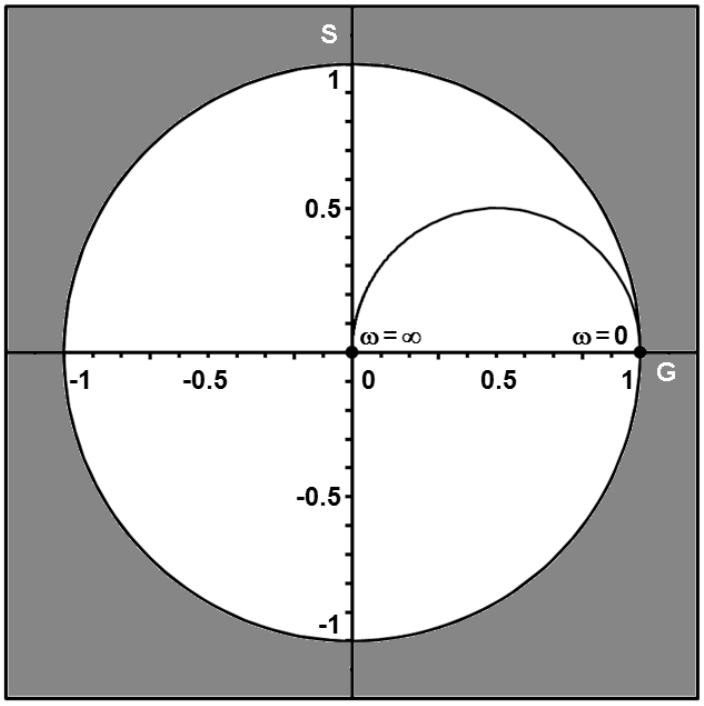

Figure 1. The phasor space (white area) and the universal semicircle.[26] Also shown are the (truly) universal points corresponding to all decay functions for zero and infinite frequencies. The universal semicircle, located in the first quadrant, defines the loci of all exponential decays. Other decay functions follow different paths between the two extreme points (ω = 0 and ω = ∞), when going from zero to infinite frequency.

For a given frequency, the (*G*, *S*) pair defines a point or, equivalently, a vector $\mathbf{P}(\omega) = G(\omega)\mathbf{e}_1 + S(\omega)\mathbf{e}_2$, called the phase vector or *phasor*. This vector is the basis of the *phasor approach* to time-resolved luminescence (mainly fluorescence),[1,4,7-26] which provides a simple graphical and model-independent portrait of a system. Besides luminophore identification ("fingerprinting") in complex systems, processes such as quenching, solvent relaxation and energy transfer are defined by characteristic trajectories in the plane (at a fixed frequency or using several frequencies). Owing to the limited computational requirements, linearity and robustness, the phasor approach is especially useful in fluorescence lifetime imaging microscopy (FLIM).[11-14,18,21,22,25] Application to measurements in homogeneous samples ("single pixel" or "in vitro" data) is nevertheless also of interest.[9,10,19,20,23]

The precise location of the decay in the plane, defined by its phasor, is a function of frequency and decay characteristics. Single exponential decays lie on a so-called *universal*

circle (in fact a semicircle, for nonnegative frequencies), defined by $S = \sqrt{G(1-G)}$, with $1 \geq G \geq 0$,[1,4,7,12-14,19] see Figure 1. Indeed, if

$$E(t) = \frac{1}{\tau}\exp\left(-\frac{t}{\tau}\right), \tag{4}$$

then eqs 2 and 3 give, as is well-known,

$$G(\omega) = \frac{1}{1+(\omega\tau)^2}, \tag{5}$$

$$S(\omega) = \frac{\omega\tau}{1+(\omega\tau)^2}. \tag{6}$$

Complex decays usually, but not always, fall inside the universal circle. The point corresponding to a multiexponential decay is located at an average distance from those of the components. In the case of a two-exponential decay with positive amplitudes, for instance, the corresponding point falls on a straight line connecting the phasors of the two components ("tie line").[1,4,7,19] Analogously to the lever rule of thermodynamic phase diagrams, the fractional contribution of each of the two components to the total intensity is given by the length of the segment connecting the decay point ("average lifetime") to the opposite component, divided by the length of the full segment uniting the two extreme points (components).[1,4,12-14,18] The lever rule was recently generalized to include cases where one of the amplitudes is negative.[26] When there are three or more components, again with positive amplitudes, the corresponding points define a polygon, with vertices located at or inside the circle, with the decay point lying in turn inside the polygon.[1,4,11-13,18] If some amplitudes are negative, the situation is different.[26]

When the measurement technique used is frequency domain fluorimetry, based on sinusoidally modulated excitation, *G* and *S* are directly related to the two parameters obtained for each frequency, which are the modulation ratio, *M*, and the phase shift, Φ, by $G = M\cos\Phi$ and by $S = M\sin\Phi$, hence $\tan\Phi = S/G$ and $M = |\mathbf{P}| = \sqrt{G^2+S^2}$ [5].

When the measurement technique used is time domain fluorimetry, the phasor must be computed (numerically or analytically) from the measured decay according to eqs 2 and 3, at a conveniently chosen frequency (or set of frequencies). This decay is often distorted by the width of the instrument response function (IRF). In order to remove its effect, the experimental decay is usually fitted with an empirical decay law, e.g. a sum of exponentials, from which the sine and cosine transforms are then computed.

The purpose of the present work is to discuss in detail the construction of the phasor plot from the time domain histogram including the effect of the instrument response function, and to test a deconvolution method in the Fourier space.

2. MATERIALS AND METHODS

Fluorescein was from Fluka (fluorescence grade, min > 98.5%) and potassium iodide (p.a.) was from Merck. The pH of the solutions was set to 9.0 with NaOH (EKA, pure). Time-resolved fluorescence intensity decays were obtained by the single-photon timing method with laser excitation and microchannel plate detection, with the set-up described in ref. 23. Excitation wavelength was 322 nm and the emission wavelength was 515 nm. The timescale was 24.4 ps/channel in the absence of KI, and 0.814 ps/channel in all other cases.

3. RESULTS AND DISCUSSION

3.1 Effect of the Instrument Response Function

When luminescence data is obtained in the time domain, namely by the single photon timing method[1] (also called time-correlated single photon counting, TCSPC), the luminescence decay is acquired directly as a histogram of photon counts, distributed by several narrow time intervals (channels). Neglecting at first the effect of the IRF on the intrinsic decay, assumed to be very short when compared to the characteristic decay times, the decay function is approximated by

$$E(t) = \sum_n f_n \delta(t - t_n), \qquad (7)$$

where

$$f_n = \frac{N_n}{\sum_n N_n}, \tag{8}$$

N_n being the number of counts in the nth channel, corresponding to time t_n. The phasor plot can be obtained directly from the histogram, as eqs 2 and 3 yield the following discrete Fourier transforms:

$$G(\omega) = \sum_n f_n \cos(\omega t_n), \tag{9}$$

$$S(\omega) = \sum_n f_n \sin(\omega t_n). \tag{10}$$

If the instrument response function $L(t)$ deviates significantly from the Dirac impulse function $\delta(t)$, then the recorded decay $R(t)$ is given by the convolution of $L(t)$ and $E(t)$,[1]

$$R(t) = \int_0^t L(u)E(t-u)\,du = L \otimes E\,. \tag{11}$$

It can be shown (by direct integration or using the Laplace transform of the convolution) that if $L(t)$ and $E(t)$ are area normalized, so is $R(t)$.

The sine and cosine Fourier transforms of $R(t)$, $G[R]$ and $S[R]$, can also be computed from the defining equations. By exchanging the integration order, performing a change of variable, and using the sum-to-product trigonometric identities for the sine and the cosine, one obtains:

$$G[R] = G[L]G[E] - S[L]S[E], \tag{12}$$

$$S[R] = S[L]G[E] + G[L]S[E]\,, \tag{13}$$

i.e., the relations retain the form of the trigonometric identities used (both follow from the product of two complex numbers, and have the form of the real and imaginary parts of that product). This system of equations can also be written in matrix form

$$\begin{bmatrix} G[R] \\ \\ S[R] \end{bmatrix} = \begin{bmatrix} G[L] & -S[L] \\ \\ S[L] & G[L] \end{bmatrix} \begin{bmatrix} G[E] \\ \\ S[E] \end{bmatrix}, \qquad (14)$$

showing that the **R** and **E** phasors are related by a linear transformation. When $L(t) = \delta(t)$ the transformation matrix reduces to the unit matrix and the **R** and **E** phasors coincide. In general, writing the **L** phasor in polar form, $G_L = M_L \cos\Phi_L$ and $S_L = M_L \sin\Phi_L$, eq 14 becomes

$$\begin{bmatrix} G[R] \\ \\ S[R] \end{bmatrix} = M_L \begin{bmatrix} \cos\Phi_L & -\sin\Phi_L \\ \\ \sin\Phi_L & \cos\Phi_L \end{bmatrix} \begin{bmatrix} G[E] \\ \\ S[E] \end{bmatrix}; \qquad (15)$$

The square matrix in eq 15 is recognized as the canonical rotation matrix[27] and therefore the transformation corresponds to a counter-clockwise rotation of the **E** phasor by Φ_L, followed by multiplication of its modulus by M_L ($M_L \leq 1$): $M_R = M_L M_E$ and $\Omega_R = \Omega_L + \Omega_E$, see Figures 2a and 3a. These results also follow from the (complex) Fourier transform of the convolution of two functions, and are indeed the basis of the frequency domain technique, where the instrument response function is a periodic function of time and $M_E = M_R/M_L$ and $\Omega_E = \Omega_R - \Omega_L$ are measured as a function of frequency. It is interesting to notice that the key frequency domain parameters (modulation and phase) have direct meaning in the time domain (phase delay and modulation ratio of the time response), while the same parameters, secondary for the time domain techniques, which are aperiodic, have direct meaning in the frequency domain (clearly appearing in the phasor plot, see Figures 2a and 3a). It is also worth remarking that the roles of the **E** and **L** phasors in the convolution are symmetric hence eqs 14 and 15 remain valid if the *L* and *E* labels are exchanged.

The above system of equations allows, in principle, computing the phasor of $E(t)$ from the measured $L(t)$ and $R(t)$ experimental histograms:

$$\begin{bmatrix} G[E] \\ \\ S[E] \end{bmatrix} = \frac{1}{G[L]^2 + S[L]^2} \begin{bmatrix} G[L] & S[L] \\ \\ -S[L] & G[L] \end{bmatrix} \begin{bmatrix} G[R] \\ \\ S[R] \end{bmatrix}, \tag{16}$$

or, equivalently,

$$\begin{bmatrix} G[E] \\ \\ S[E] \end{bmatrix} = \frac{1}{M_L} \begin{bmatrix} \cos\Phi_L & \sin\Phi_L \\ \\ -\sin\Phi_L & \cos\Phi_L \end{bmatrix} \begin{bmatrix} G[R] \\ \\ S[R] \end{bmatrix}, \tag{17}$$

corresponding, not unexpectedly at this point, to a clockwise rotation of the **R** phasor by Φ_L, followed by division of its modulus by M_L ($M_L \leq 1$), thus restoring the **E** phasor:[19] $M_E = M_R/M_L$ and $\Omega_E = \Omega_R - \Omega_L$, see Figures 2a and 3a. Equations 16-17 represent therefore a deconvolution in the Fourier space.

As mentioned, eqs 14 and 15 remain valid if the *L* and *E* labels are exchanged. In this way, one also obtains,

$$\begin{bmatrix} G[L] \\ \\ S[L] \end{bmatrix} = \frac{1}{G[E]^2 + S[E]^2} \begin{bmatrix} G[E] & S[E] \\ \\ -S[E] & G[E] \end{bmatrix} \begin{bmatrix} G[R] \\ \\ S[R] \end{bmatrix}, \tag{18}$$

$$\begin{bmatrix} G[L] \\ \\ S[L] \end{bmatrix} = \frac{1}{M_E} \begin{bmatrix} \cos\Phi_E & \sin\Phi_E \\ \\ -\sin\Phi_E & \cos\Phi_E \end{bmatrix} \begin{bmatrix} G[R] \\ \\ S[R] \end{bmatrix}. \tag{19}$$

These relations allow computing the Fourier cosine and sine transforms of the IRF, by using a fluorescence standard of known lifetime, whose response is measured at the sample emission wavelength, thus avoiding the color effect (when significant).[1] In terms of phase and modulation, the relations for the computation of the **E** phasor become $\Omega_E = \Omega_E^* + \Omega_R - \Omega_R^*$ and $M_E = \left(\frac{M_R}{M_R^*}\right) M_E^*$, where the asterisk refers to the standard. The parameters Ω_R^* and M_R^* are

measured experimentally, while Ω_E^* and M_E^* are computed for each frequency. These results can also be derived by combining the (complex) Fourier transforms of $R = L \otimes E$ and of $R^* = L \otimes E^*$.

3.2 Model Calculations

3.2.1 Rectangular impulse

To discuss the effect of the IRF on the phasor plot, an exponential decay function, eq 1, will be used. The simplest IRF is the rectangular impulse (area normalized and starting at $t = 0$) of width Δt and height $1/\Delta t$. Its cosine and sine transforms are

$$G_L(\omega) = \frac{\sin(\omega \Delta t)}{\omega \Delta t}, \tag{20}$$

$$S_L(\omega) = \frac{1 - \cos(\omega \Delta t)}{\omega \Delta t}. \tag{21}$$

The respective phasor plot has an interesting shape, see Figure 2b, crossing the origin an infinite number of times. This curve is known as the cochleoid («snail-shaped»).[28] It can also be said to be universal, in the sense that it describes all rectangular pulses. The respective phasor position for a given frequency is a function of the product $\omega \Delta t$. Short pulses lag behind the exponential decay phasor, see Figure 2a, and may even stay close to the point (1,0) for most or all experimental frequencies (thus approaching delta pulse excitation). On the other hand, the phasor of a broad pulse (compared to the lifetime) precedes the phasor of the exponential decay and traces most of the curve in the same range of frequencies, see Figures 3a and 3b.

The "decay" $R(t)$, given by eq 11, is

$$R(t) = \begin{cases} \frac{1}{\Delta t}\left(1 - e^{-t/\tau}\right) & \text{if} \quad t < \Delta t \\ \\ \frac{1}{\Delta t}\left(e^{\Delta t/\tau} - 1\right) e^{-t/\tau} & \text{if} \quad t \geq \Delta t \end{cases} \tag{22}$$

and in fact displays a rise time, corresponding to the buildup period.

The respective Fourier cosine and sine transforms can be obtained either directly or using eqs 12 and 13, together with eqs 5, 6, 20 and 21 to give, in the form of eq 14,

$$\begin{bmatrix} G_R(\omega) \\ S_R(\omega) \end{bmatrix} = \begin{bmatrix} \dfrac{\sin(\omega\Delta t)}{\omega\Delta t} & -\dfrac{1-\cos(\omega\Delta t)}{\omega\Delta t} \\ \dfrac{1-\cos(\omega\Delta t)}{\omega\Delta t} & \dfrac{\sin(\omega\Delta t)}{\omega\Delta t} \end{bmatrix} \begin{bmatrix} \dfrac{1}{1+(\omega\tau)^2} \\ \dfrac{\omega\tau}{1+(\omega\tau)^2} \end{bmatrix}. \qquad (23)$$

Defining a reduced frequency $u = \omega\tau$ and a ratio $\gamma = \Delta t/\tau$, eq 21 becomes:

$$\begin{bmatrix} G_R(u) \\ S_R(u) \end{bmatrix} = \begin{bmatrix} \dfrac{\sin(\gamma u)}{\gamma u} & -\dfrac{1-\cos(\gamma u)}{\gamma u} \\ \dfrac{1-\cos(\gamma u)}{\gamma u} & \dfrac{\sin(\gamma u)}{\gamma u} \end{bmatrix} \begin{bmatrix} \dfrac{1}{1+u^2} \\ \dfrac{u}{1+u^2} \end{bmatrix} \qquad (24)$$

The effect of parameter γ on the phasor plots is shown in Figures 2 and 3. In Figure 2a the effect of the IRF $L(t)$ on the decay is exemplified for $\gamma = 0.5$: At a given frequency ($u = 1$), the convolution with $L(t)$ increases the phase with respect to that of $E(t)$ and reduces the modulation (in the example, the reduction is small, as M_L, although smaller than 1, is still very close to 1, see Figure 2d). In Figure 2b the full phasor plot is shown for the same γ. Owing to the initial rise time, the phasor plot of the response $R(t)$ occurs outside the universal circle, and crosses the third quadrant for high frequencies (see zoom in Figure 2c).

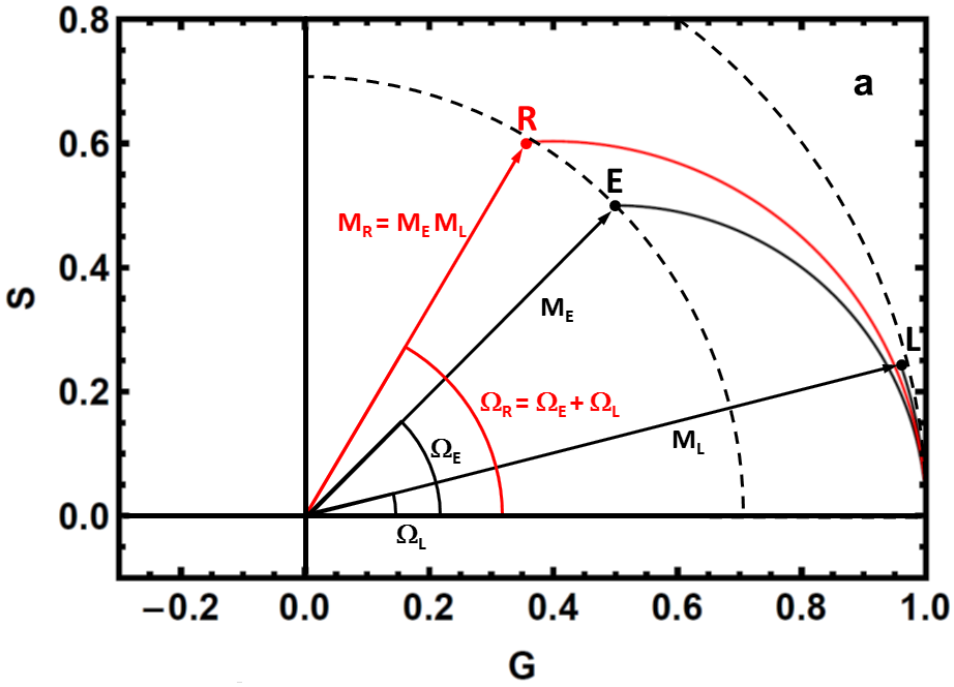
a
R
E
L
$M_R = M_E M_L$
M_E
M_L
$\Omega_R = \Omega_E + \Omega_L$
Ω_E
Ω_L
S
G
0.8
0.6
0.4
0.2
0.0
−0.2
0.0
0.2
0.4
0.6
0.8
1.0

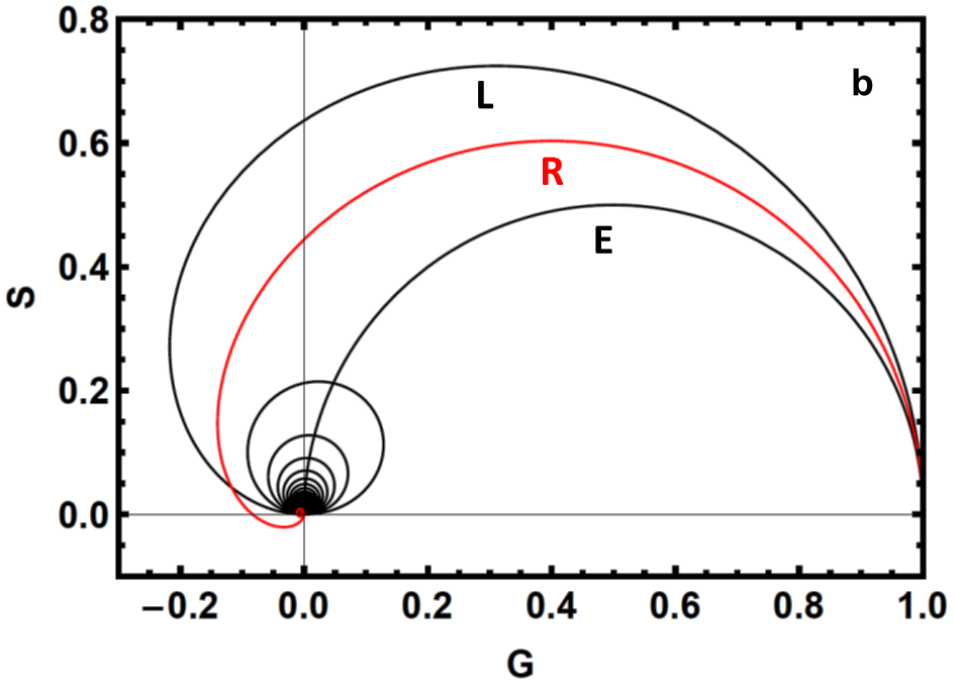
b
L
R
E
S
G
0.8
0.6
0.4
0.2
0.0
−0.2
0.0
0.2
0.4
0.6
0.8
1.0

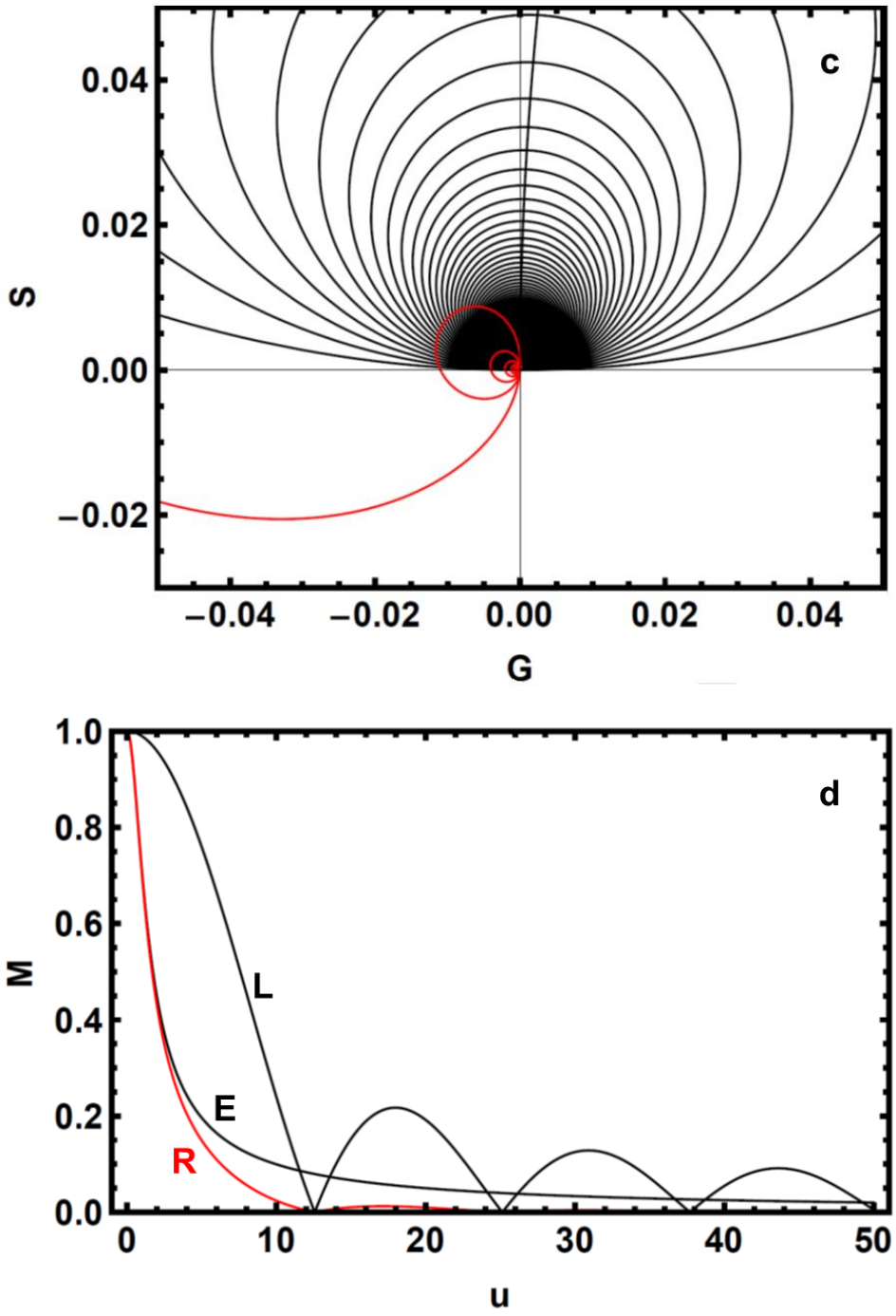

Figure 2. Phasor plots for a decay resulting from the convolution of a rectangular impulse with an intrinsically exponential decay, according to eqs 20 - 24. The reduced parameter is $\gamma = \Delta t/\tau = 0.5$. In (**a**) the reduced frequency is $u = 1$. In (**b**), the full curves are shown as a function of frequency. (**c**) is a zoom of (**b**) near the origin. For large frequencies the **R** phasor can be viewed as the **L** phasor rotated by 90º and multiplied by M_E. In (**d**) the modulation of the three phasors is shown as a function of the reduced frequency.

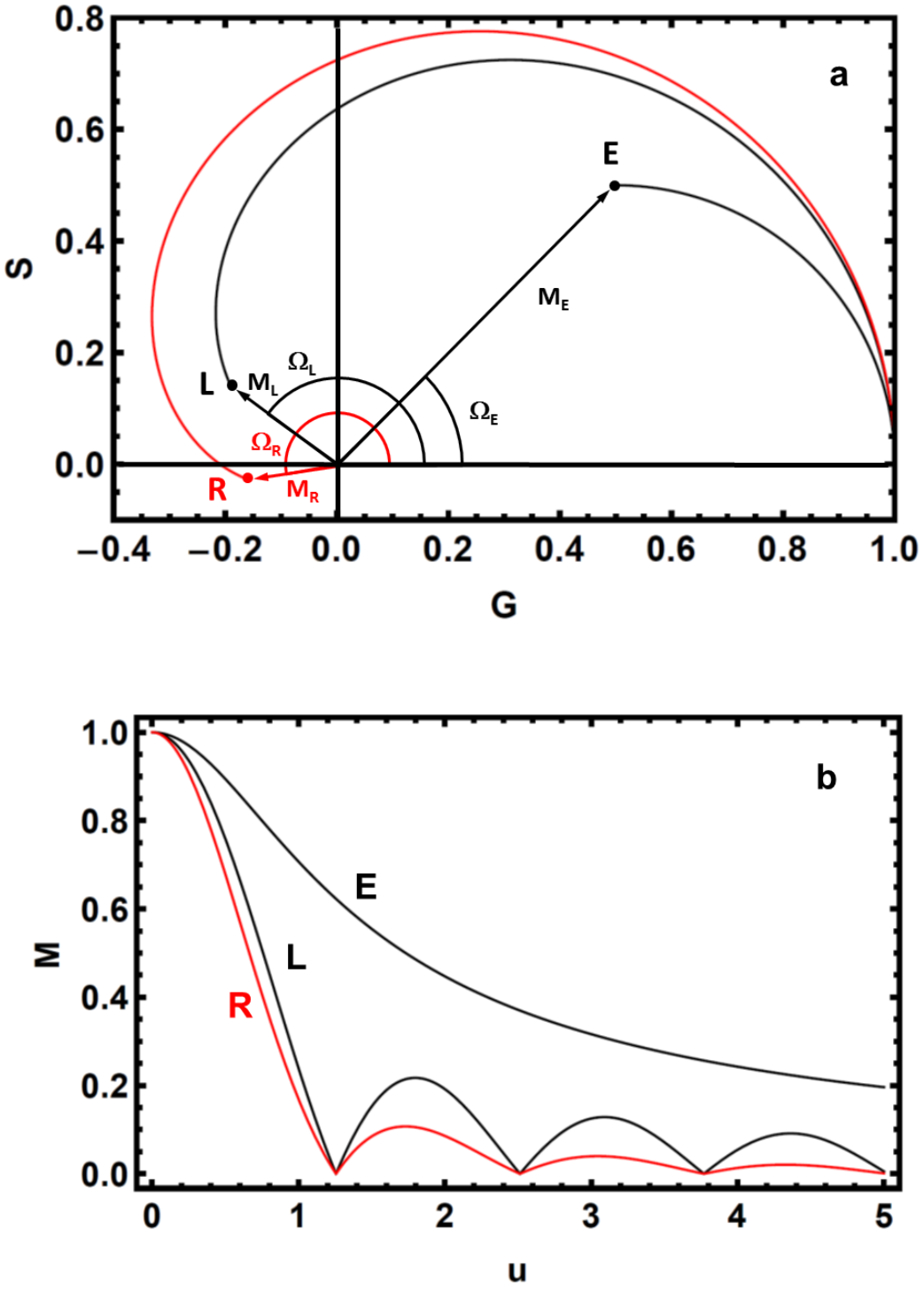

Figure 3. As in Figure 2, but now with a broader impulse, $\gamma = 5$. In (**a**) the reduced frequency is $u = 1$. In (**b**), the modulation of the three phasors is shown as a function of the reduced frequency.

In Figure 4 it is seen that the departure from the universal circle is the bigger the larger is γ, as expected. It is observed (not shown) that the deviations are essentially negligible for $\gamma < 0.01$.

One may thus expect that using an IRF with FWHM of 40 ps, no deconvolution will be necessary for plotting phasors corresponding to lifetimes higher than about 4 ns. This is a much more stringent condition than the one imposed in the time domain, and results from the fact that Fourier transformation involves an integration over time, while for a time domain analysis the very first part of the decay (which contributes more than proportionally to the integral in the case of a monotonic decay), can nevertheless be neglected (in the absence of transient effects).

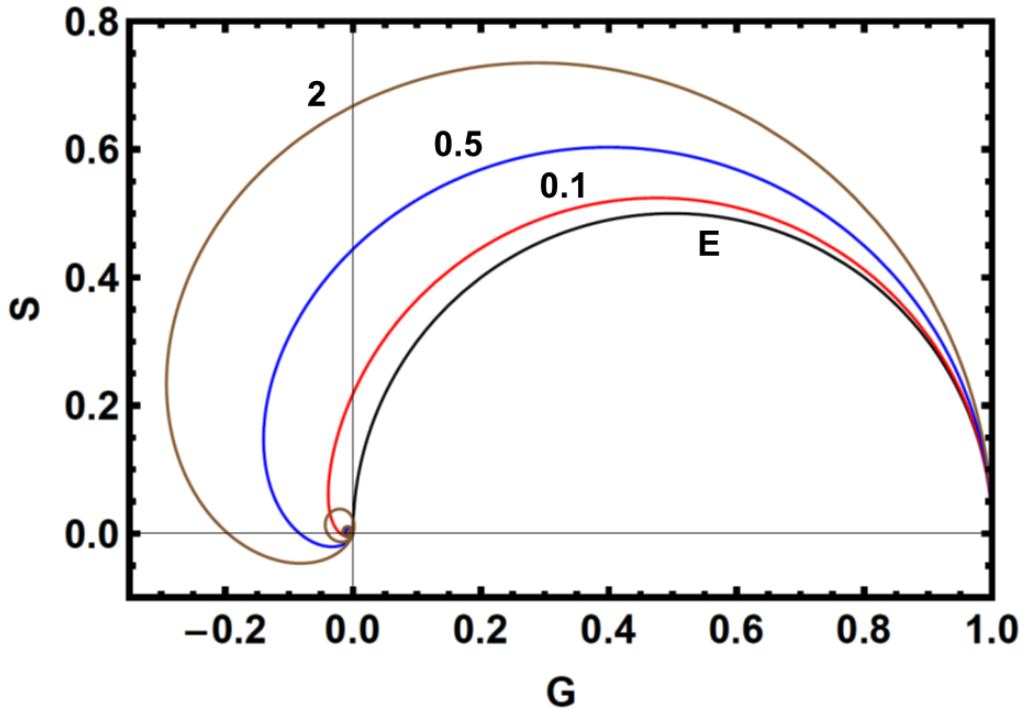

Figure 4. Phasor plots of the response **R** for a decay resulting from the convolution of a rectangular impulse with an intrinsically exponential decay, as a function of the reduced parameter $\gamma = \Delta t/\tau$. The values of γ are shown next to each curve.

3.2.2 Gamma impulse

A more realistic shape is now considered for the normalized IRF: a gamma probability density function,

$$L(t) = \frac{1}{\beta\Gamma(\alpha)}\left(\frac{t}{\beta}\right)^{\alpha-1}\exp\left(-\frac{t}{\beta}\right), \qquad (25)$$

where α and β are respectively shape and scale parameters, and $\Gamma(x)$ is the gamma function. The gamma IRF, whose mean and standard deviation are $\beta\alpha$ and $\beta\sqrt{\alpha}$, respectively, has a tail, which is the main problem in practical deconvolution. Were the IRF a strict rectangular pulse and the analysis would be very simple, just by starting it immediately after the end of the pulse.

The cosine and sine transforms of eq 25 are

$$G_L(\omega) = \frac{\cos\left[\alpha \arctan(\beta\omega)\right]}{\left[1+(\beta\omega)^2\right]^{\frac{\alpha}{2}}}, \tag{26}$$

$$S_L(\omega) = \frac{\sin\left[\alpha \arctan(\beta\omega)\right]}{\left[1+(\beta\omega)^2\right]^{\frac{\alpha}{2}}}. \tag{27}$$

The respective phasor plot is spiral-shaped under some conditions, see Figure 5.

The "decay" $R(t)$, again with a rise time and given by eq 11, has no simple explicit form. However, the respective Fourier cosine and sine transforms can be directly obtained e.g. using eq 14 together with eqs 5, 6, 26 and 27 to give:

$$\begin{bmatrix} G_R(\omega) \\ S_R(\omega) \end{bmatrix} = \begin{bmatrix} \frac{\cos\left[\alpha \arctan(\beta\omega)\right]}{\left[1+(\beta\omega)^2\right]^{\frac{\alpha}{2}}} & -\frac{\sin\left[\alpha \arctan(\beta\omega)\right]}{\left[1+(\beta\omega)^2\right]^{\frac{\alpha}{2}}} \\ \frac{\sin\left[\alpha \arctan(\beta\omega)\right]}{\left[1+(\beta\omega)^2\right]^{\frac{\alpha}{2}}} & \frac{\cos\left[\alpha \arctan(\beta\omega)\right]}{\left[1+(\beta\omega)^2\right]^{\frac{\alpha}{2}}} \end{bmatrix} \begin{bmatrix} \frac{1}{1+(\omega\tau)^2} \\ \frac{\omega\tau}{1+(\omega\tau)^2} \end{bmatrix}, \tag{28}$$

Defining a reduced frequency $u = \omega\tau$ and a ratio $\gamma = \beta/\tau$, eq 28 becomes:

$$\begin{bmatrix} G_R(u) \\ S_R(u) \end{bmatrix} = \begin{bmatrix} \dfrac{\cos\left[\alpha \arctan(\gamma u)\right]}{\left[1+(\gamma u)^2\right]^{\frac{\alpha}{2}}} & -\dfrac{\sin\left[\alpha \arctan(\gamma u)\right]}{\left[1+(\gamma u)^2\right]^{\frac{\alpha}{2}}} \\ \dfrac{\sin\left[\alpha \arctan(\gamma u)\right]}{\left[1+(\gamma u)^2\right]^{\frac{\alpha}{2}}} & \dfrac{\cos\left[\alpha \arctan(\gamma u)\right]}{\left[1+(\gamma u)^2\right]^{\frac{\alpha}{2}}} \end{bmatrix} \begin{bmatrix} \dfrac{1}{1+u^2} \\ \dfrac{u}{1+u^2} \end{bmatrix}. \quad (29)$$

The effect of the gamma impulse position and width on the phasor plot is shown in Figures 5 and 6. The key parameters are the impulse dimensionless average value, $p = \dfrac{\alpha\beta}{\tau} = \alpha\gamma$, and the dimensionless standard deviation of the impulse, given by $w = \dfrac{\beta\sqrt{\alpha}}{\tau} = \gamma\sqrt{\alpha}$. Narrow impulses, when not centered at the origin of times, result in a spiraling phasor, see Figures 5a and 5b. The extreme case corresponds to $L(t) = \delta(t\text{-}t_0)$ which has $G_L(\omega) = \cos(\omega t_0)$ and $S_L(\omega) = \sin(\omega t_0)$, which is in turn an example of the shift property of causal functions.[29]

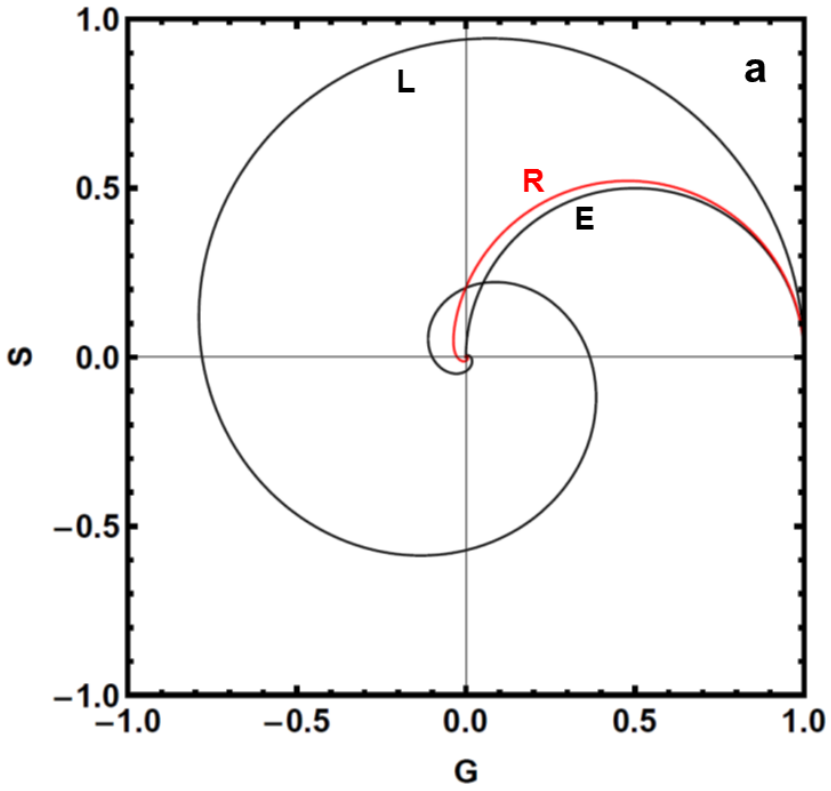

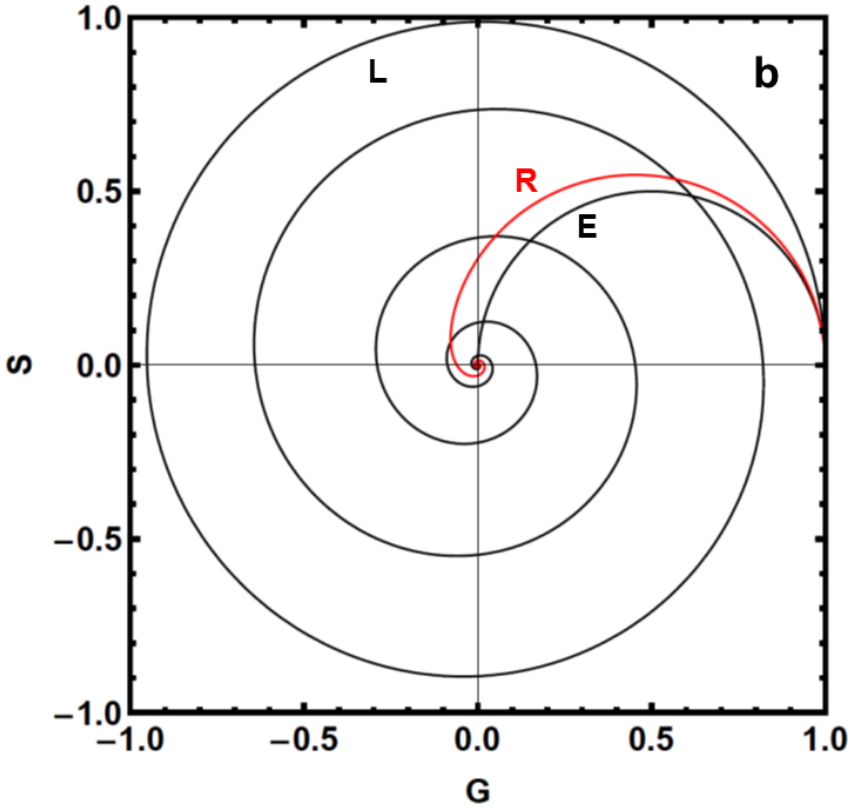

Figure 5. Phasor plots for a decay resulting from the convolution of a gamma impulse with an intrinsically exponential decay, according to eqs 26 - 29. Reduced parameters are: p = 0.044 and w = 0.01 (α = 20 and γ = 0.0022) (**a**), p = 0.1 and w = 0.01 (α = 100 and γ = 0.001) (**b**).

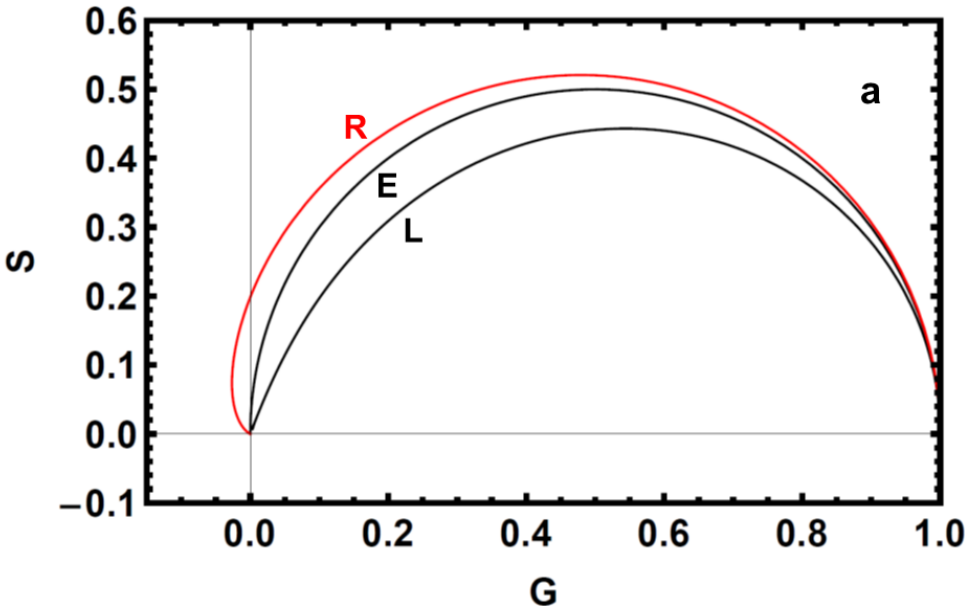

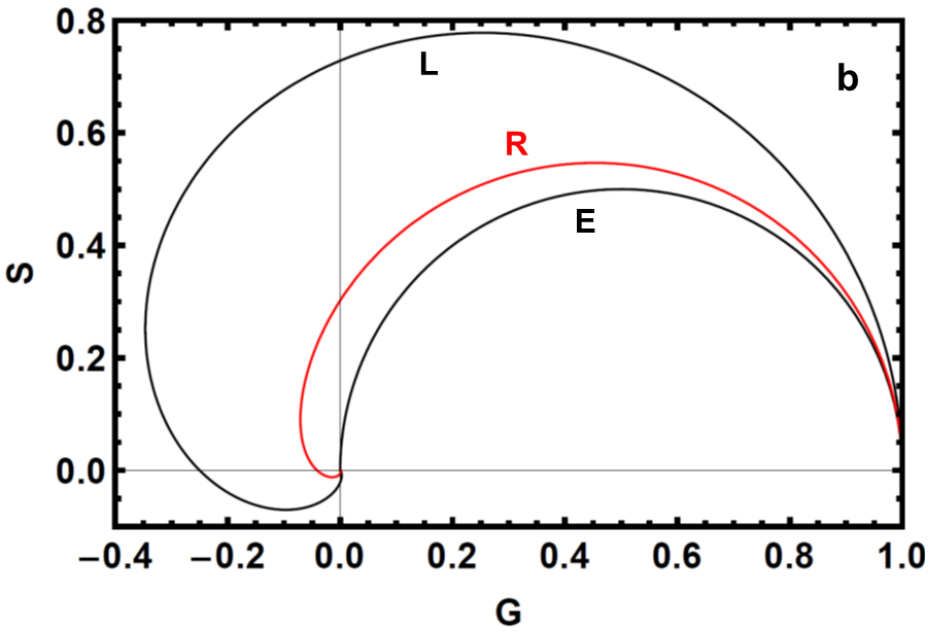

Figure 6. As in Figure 5, but now with p = 0.044 and w = 0.05 (α = 0.77 and γ = 0.057) (**a**), p = 0.1 and w = 0.05 (α = 4 and γ = 0.025) (**b**).

3.3 Analysis of Real Data

In order to complement and check the applicability of the theoretical results obtained in Section 3.2, the fluorescence decays of dilute alkaline (pH 9) aqueous solutions of fluorescein (3×10^{-5} M) were measured as a function of potassium iodide concentration (2, 4, 6 and 8 M, see Table 1). The decay of fluorescein in the absence of iodide is single exponential with a lifetime of 4.2 ns, in agreement with the published value.[1] The decay of fluorescein in the presence of the concentrated quencher is close to single exponential up to 2 M (leading to a collisional quenching rate constant of 2×10^{9} M^{-1} s^{-1}), but becomes more complex above this concentration, see Table 1.

Table 1. Fluorescein decay analysis with a sum of exponentials for several concentrations of KI. The fractional steady-state intensities f_i are given in parenthesis.

KI/M	τ_1/ps (%)	τ_2/ps (%)	τ_3/ps (%)	τ_{av}/ps
0	4240 (100)	-	-	4240
2.0	95 (5.7)	274 (94.3)	-	264
4.0	45 (11.5)	116 (88.5)	-	108
6.0	30 (24.8)	78 (75.2)	-	66
8.0	0.5 (3.0)	34 (79.4)	72 (17.6)	40

A representative decay (2 M KI) and the corresponding two-exponential fit are shown in Figure 7.

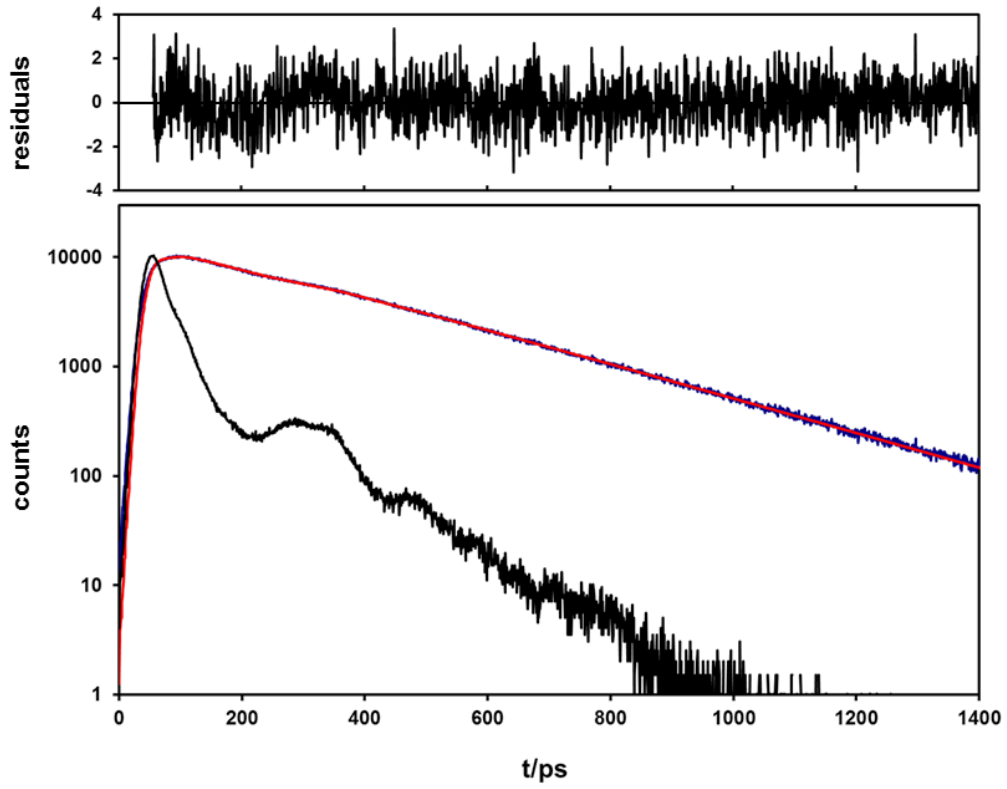

Figure 7. Fluorescence decay of fluorescein in the presence of 2 M KI, and fit with a sum of two exponentials (reduced chi-squared = 1.03), see Table 1.

The Fourier cosine and sine transforms of the experimental decay (*R*), computed according to eqs 9 and 10, are shown in Figure 8 as a function of frequency for all KI concentrations. Very significant differences are observed between these curves and the respective **E** curves (same color, but dashed), computed with eqs 30 and 31 and using the parameters given in Table 1,

$$G_E(\omega) = \sum_i f_i \frac{1}{1+(\omega\tau_i)^2}, \tag{30}$$

$$S_E(\omega) = \sum_i f_i \frac{\omega\tau_i}{1+(\omega\tau_i)^2}. \tag{31}$$

The **E** phasor plots for all KI solutions clearly depart from the universal semicircle, falling deeper in the sub-exponential region as the concentration increases [26]. It also seen in Figure 8 that the IRF impact on the **R** phasor plot is the more important, the shortest the fluorescence average decay time, as expected. Notwithstanding the fact that the IRF has a FWHM of 39 ps, even the **R** phasor plot of fluorescein in the absence of KI (4.2 ns lifetime) differs from the respective **E** phasor plot.

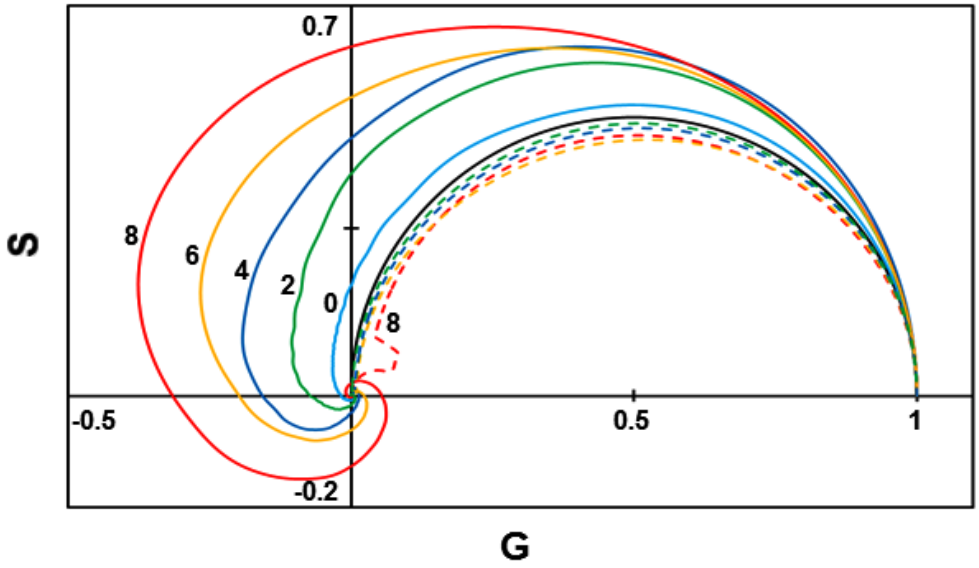

Figure 8. Phasor plots of the experimental decays of fluorescein (**R**) as a function of KI concentration (values next to each curve, in M units). Also shown are the corresponding **E** phasor plots (dashed) computed with eqs 30 and 31. The **E** phasor plot corresponding to fluorescein in the absence of KI coincides with the universal circle (black solid line).

Deconvolution in the Fourier space using eq 16 was attempted for the entire series of fluorescein solutions. Very good results were obtained for the 0 M (pure fluorescein) and 2 M KI solutions, but they were not so good for the more concentrated KI solutions. A similar pattern was observed for a second set of solutions, using NaI instead of KI (up to 12 M, as NaI has a higher solubility). Recovery of the intrinsic phasor curves (**E**) from the experimental decay (**R**) and IRF (**L**) phasors was indeed found to be sensitive to the relative position of the IRF and decay (time shift) for fast decays, and thus becomes problematic for very short lifetimes. However, the method works well for lifetimes at least one order of magnitude higher than the IRF time width, which is the most common situation.

The deconvolution for fluorescein in the absence of KI is depicted in Figure 9. It is seen that the universal circle curve corresponding to a single exponential decay (**E**) is perfectly recovered from the experimental decay phasor (**R**). The position of the three phasors is shown for a frequency of 38 MHz that gives the maximum *S* value of the universal circle (*S* = 0.5) for the fluorescein lifetime (4.2 ns). Similar results (not shown), including the successful recovery of the intrinsic phasor (**E**), were obtained for a solution of POPOP in ethanol, which has a single exponential fluorescence decay with a lifetime of 1.2 ns.[23]

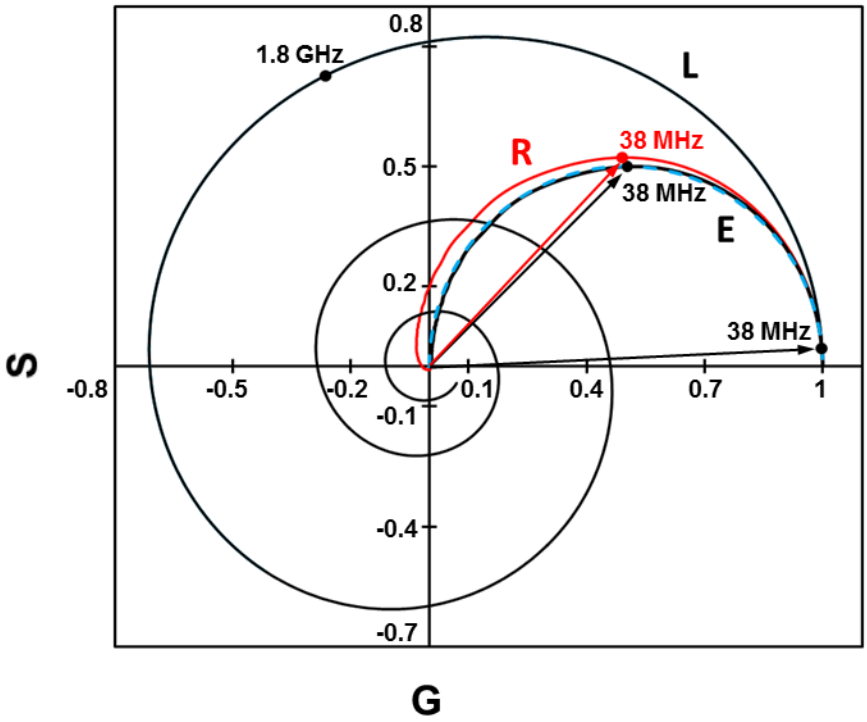

Figure 9. Plots of the **L**, **R** and **E** phasors for fluorescein in the absence of KI. The computed **E** phasor plot (dashed) coincides with the universal circle (black solid line), in agreement with a single exponential decay. An upper frequency of 1.8 GHz suffices to define the full **E** curve. The position of the **L** phasor is shown for this frequency. Cf. Figure 2A for the relative position of the three phasors.

The deconvolution for fluorescein in the presence of 8 M KI is shown in Figure 10. Note the different shape of the **L** phasor for very high frequencies with respect to Figure 9. This difference, not relevant for the analysis, results from the fact that the time scale is not the same in the two cases. The **E** phasor plot computed with eqs 30 and 31 (blue solid line) does not coincide with the universal circle (black solid line), as expected for a subexponential decay (see

Table 1). The deconvolved **E** phasor (blue dashed line) lies close to but does not coincide exactly with the curve computed with eqs 30 and 31 (blue solid line).

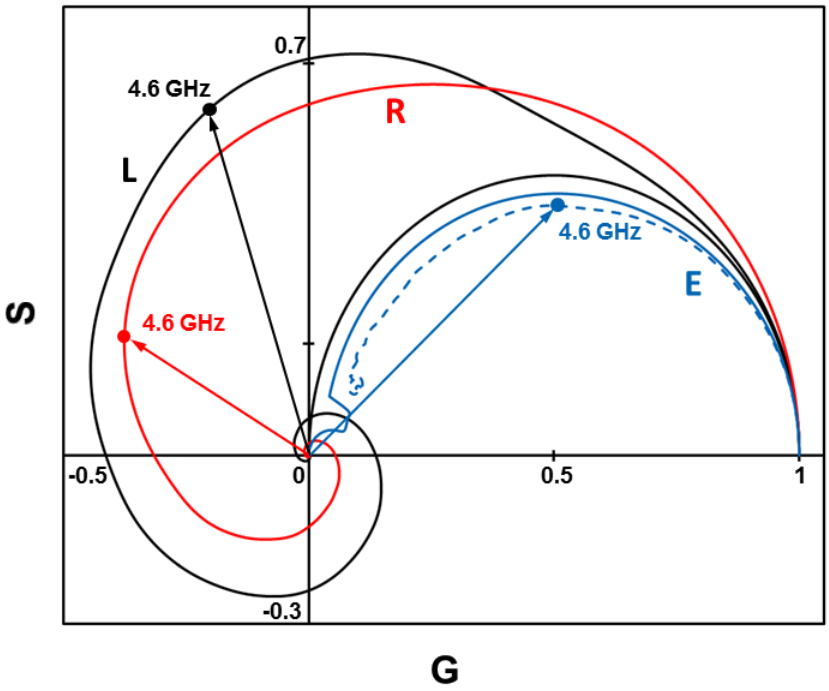

Figure 10. Plots of the **L**, **R** and **E** phasors for fluorescein in the presence of 8 M KI. The deconvolved **E** phasor (blue dashed line) does not coincide exactly with the **E** phasor plot computed with eqs 30 and 31 (blue solid line). The universal circle is also shown (black solid line). Cf. Figure 3a for the relative position of the three phasors.

4. CONCLUSIONS

The construction of the fluorescence phasor plot from time domain experimental data was discussed, including the effect of the instrument response function that was given a geometrical interpretation. Calculations were performed for model impulses, and a deconvolution method in the Fourier space described. Fluorescein decays in the absence and presence of KI were converted into phasor plots and analyzed by the methods introduced. The effect of the impulse was clearly shown, in accordance with model predictions. Deconvolution in the Fourier space works well for lifetimes at least one order of magnitude higher than the IRF time width.

ACKNOWLEDGEMENTS

This work was carried out within projects PTDC/QUI-QUI/123162/2010 and RECI/CTM-POL/0342/2012 (FCT, Portugal).

REFERENCES

(1) Valeur B.; Berberan-Santos, M. N. Molecular *Fluorescence. Principles and Applications*, 2nd ed.; Wiley-VCH: Weinheim, 2012.

(2) Valeur B.; Berberan-Santos, M. N. Luminescence Decays with Underlying Distributions: General Properties and Analysis with Mathematical Functions. *J. Lumin.* **2007**, *126*, 263-272.

(3) Papoulis, A. *The Fourier Integral and its Applications*; McGraw-Hill: New York, 1962.

(4) Jameson, D. M. *Introduction to Fluorescence*; CRC Press: Boca Raton, 2014.

(5) Weber, G. Resolution of the Fluorescence Lifetimes in a Heterogeneous System by Phase and Modulation Measurements. *J. Phys. Chem.* **1981**, *85*, 949-953.

(6) Feller, W. *An Introduction to Probability Theory and its Applications*, vol. II, 2nd. ed.; Wiley: New York, 1971.

(7) Jameson, D. M.; Gratton, E.; Hall, R. D. The Measurement and Analysis of Heterogeneous Emissions by Multifrequency Phase and Modulation Fluorometry. *Appl. Spectrosc. Rev.* **1984**, *20*, 55-106.

(8) Berberan-Santos, M. The Time Dependence of Rate Coefficients and Fluorescence Anisotropy for Non-delta Production. *J. Lumin.* **1991**, *50*, 83-87.

(9) Itagaki, M.; Watanabe, K. Determination of Fluorescence Lifetime with Transfer Function Processed by Fast Fourier Transformation. *Bunseki Kagaku* **1994**, *43*, 1143-1148.

(10) Itagaki, M.; Hosono, M.; Watanabe, K. Analysis of Pyrene Fluorescence Emission by Fast Fourier Transformation. *Anal. Sci.* **1997**, *13*, 991-996.

(11) Verveer, P. J.; Bastiaens, P. I. H. Evaluation of Global Analysis Algorithms for Single Frequency Fluorescence Lifetime Imaging Microscopy Data. *J. Microsc.* **2003**, *209*, 1-7.

(12) Clayton, A. H. A.; Hanley, Q. S.; Verveer, P. J. Graphical Representation and Multicomponent Analysis of Single-frequency Fluorescence Lifetime Imaging Microscopy Data. *J. Microsc.* **2004**, *213*, 1-5.

(13) Redford, G. I.; Clegg, R. M. Polar Plot Representation for Frequency-Domain Analysis of Fluorescence Lifetimes. *J. Fluoresc.* **2005**, *15*, 805-815.

(14) Digman, M. A.; Caiolfa, V. R.; Zamai, M.; Gratton, E. The Phasor Approach to Fluorescence Lifetime Imaging Analysis. *Biophys. J.* **2008**, *94*, L14-L16.

(15) Clayton, A. H. A. The Polarized AB Plot for the Frequency-domain Analysis

and Representation of Fluorophore Rotation and Resonance Energy Homotransfer. *J. Microsc.* **2008**, *232*, 306-312.
(16) Chen, Y.-C.; Clegg, R. M. Fluorescence Lifetime-resolved Imaging. *Photosynth. Res.* **2009**, *102*, 143-155.
(17) Chen, Y.-C.; Spring, B. Q.; Buranachai, C.; Malachowski, G.; Clegg, R. M. What is Behind All Those Lifetimes Anyway? Where Do We Go from Here? *Proc. SPIE* **2009**, *7183*, 718302.
(18) Stringari, C.; Cinquin, A.; Cinquin, O.; Digman, M. A.; Donovan, P. J.; Gratton, E. Phasor Approach to Fluorescence Lifetime Microscopy Distinguishes Different Metabolic States of Germ Cells in a Live Tissue, *Proc. Natl. Acad. Sci. U.S.A.* **2011**, *108*, 13582-13587.
(19) Stefl, M.; James, N. G.; Ross, J.A.; Jameson, D. M. Applications of Phasors to in vitro Time-resolved Fluorescence Measurements. *Anal. Biochem.* **2011**, *410*, 62-69.
(20) James, N. G.; Ross, J. A.; Stefl, M.; Jameson, D. M. Applications of Phasor Plots to in vitro Protein Studies. *Anal. Biochem.* **2011**, *410*, 70-76.
(21) Hinde, E.; Digman, M. A.; Welch, C.; Hahn, K. M.; Gratton, E. Biosensor Förster Resonance Energy Transfer Detection by the Phasor Approach to Fluorescence Lifetime Imaging Microscopy. *Microsc. Res. Tech.* **2012**, *75*, 271-281.
(22) Digman M. A.; Gratton, E. in *Fluorescence Lifetime Spectroscopy and Imaging: Principles and Applications in Biomedical Diagnostics*, Marcu, L.; French, P. M. W.; Elson, D. S., eds.; CRC Press: Boca Raton, 2012.
(23) Menezes, F.; Fedorov, A.; Baleizao, C.; Valeur, B.; Berberan-Santos, M. N. Methods for the Analysis of Complex Fluorescence Decays: Sum of Becquerel Functions versus Sum of Exponentials. *Methods Appl. Fluoresc.* **2013**, *1*, 015002.
(24) Hinde, E.; Digman, M. A.; Hahn, K. M.; Gratton, E. Millisecond Spatiotemporal Dynamics of FRET Biosensors by the Pair Correlation Function and the Phasor Approach to FLIM. *Proc. Natl. Acad. Sci. U.S.A.* **2013**, *110*, 135-140.
(25) Engelborghs, Y.; Visser A. J. W. G., eds., *Fluorescence Spectroscopy and Microscopy*; Humana Press: New York, 2014.
(26) Berberan-Santos, M. N. Phasor Plots of Luminescence Decay Functions. *Chem. Phys.* **2015**, *449*, 23-33.
(27) McQuarrie, D. A. *Mathematical Methods for Scientists and Engineers*; University Science Books: Sausalito, 2003.

(28) Lawrence, J. D. *A Catalogue of Special Plane Curves*; Dover: Mineola, 1972.
(29) Berberan-Santos, M. N. Probabilistic View of the Luminescence Phasor Plot and Description of the Universal Semicircle as the Sum of Two Spiraling Curves. *J. Math. Chem.* **2015**, 53, 1207-1219.

TOC Graphical Abstract